J|A|C|S
ARTICLES
Published on Web 02/19/2002

Theoretical Determination of Chromophores in the Chromogenic Effects of Aromatic Neurotoxicants

Chang-Guo Zhan,[†] David A. Dixon,*,[†] Mohammad I. Sabri,[‡] Min-Sun Kim,[‡] and Peter S. Spencer[‡]

Contribution from Theory, Modeling & Simulation, William R. Wiley Environmental Molecular Sciences Laboratory, Pacific Northwest National Laboratory, MS K1-83, P.O. Box 999, Richland, Washington 99352, and Center for Research on Occupational and Environmental Toxicology, Oregon Health Sciences University, 3181 S.W. Sam Jackson Park Road L606, Portland, Oregon 97201

Received May 31, 2001

Abstract: We report the first computational study of the chromophores responsible for the chromogenic effects of aromatic neurotoxicants containing a 1,2-diacetyl moiety in their oxidation metabolites. A series of ab initio electronic structure calculations was performed on two representative aromatic compounds, 1,2-diacetylbenzene (1,2-DAB) and 1,2-diacetyl tetramethyl tetralin (1,2-DATT), the putative active metabolites of the neurotoxic aromatic hydrocarbon compounds 1,2-diethylbenzene (1,2-DEB) and acetyl ethyl tetramethyl tetralin (AETT), and on the products of their possible reactions with proteins that result in chromogenic effects. The electronic excitation energies determined by three different computational approaches were found to be consistent with each other. The calculated results are consistent with the conclusion/prediction that the chromogenic effects of 1,2-DAB (or 1,2-DEB) and 1,2-DATT (or AETT) could result from ninhydrin-like reactions, rather than the formation of pyrrole-like compounds. Our pK_a calculations further indicate that the chromophore, i.e., the product of the ninhydrin-like reaction showing the blue color, is deprotonated in neutral aqueous solution. The corresponding protonated structure has a different color as it absorbs in the blue region of the visible spectrum, and its chromogenic contribution would be significant in solution at low pH.

Introduction

Chromogenic aromatic hydrocarbon compounds are present in fuels and solvents and, formerly, in consumer products; they also occur in contaminated soil and water at hazardous waste sites.[1] That certain aromatic hydrocarbons exhibit chromogenic and neurotoxic behavior has been known for a number of years, where we define a chromogenic speices as one that is colored and can be observed. In 1979, Spencer et al.[2] described the remarkable chromogenic and neurotoxic effects of acetyl ethyl tetramethyl tetralin (AETT, **3** in Scheme 1), a fragrance raw material and food additive that was subsequently removed from consumer products.[3] Tetralin itself, and a number of other dicyclic and monocyclic aromatic hydrocarbon compounds, have chromogenic properties in humans and/or animals, but they have not been tested for neurotoxicity.[3]

1,2-Diethylbenzene (1,2-DEB, **1** in Scheme 1) is one of the simplest representatives of the chromogenic and neurotoxic aromatic hydrocarbon compounds.[4] This organic solvent produces chromogenic and neurotoxic effects through its oxidation metabolite 1,2-diacetylbenzene (1,2-DAB, **2** in Scheme 1).[5] In a similar fashion, AETT exerts its chromogenic and neurotoxic effects through its presumed metabolite, 1,2-diacetyl tetramethyl tetralin (1,2-DATT, **4** in Scheme 1).[3] Thus, 1,2-DAB and 1,2-DATT, which are colorless as shown below, have a common 1,2-diacetyl moiety and display similar chromogenic properties. They form blue pigments on contact with proteins, skin, and other tissues.[6,7] Rodents treated systemically with 1,2-DEB, 1,2-

Scheme 1

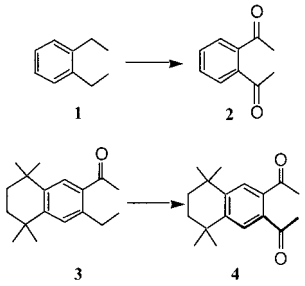

* Corresponding author.
† Pacific Northwest National Laboratory.
‡ Oregon Health Sciences University.

(1) Johnson, B. L.; DeRosa, C. T. *Rev. Environ. Health* **1997**, *12*, 235.
(2) Spencer, P. S.; Sterman, A. B.; Horoupian, D. S.; Folds, M. N. *Science* **1979**, *204*, 633.
(3) Spencer, P. S.; Folds, M. N.; Sterman, A. B.; Horoupian, D. S. In *Experimental and Clinical Neurotoxicology*; Spencer, P. S., Schaumburg, H. H., Eds.; Williams and Wilkins: Baltimore, 1980; p 296.
(4) Gagnaire, F.; Marignac, B.; de Ceaurriz, J. *J. Appl. Toxicol.* **1990**, *10*, 105.
(5) Gagnaire, F.; Ensminger, A.; Marignac, B.; de Ceaurriz, J. *J. Appl. Toxicol.* **1991**, *11*, 261.
(6) Spencer, P. S. In *Experimental and Clinical Neurotoxicology*, 2nd ed.; Spencer, P. S., Schaumburg, H. H., Eds.; Oxford University Press: New York, 2000; p 112.
(7) Kim, M.-S.; Sabri, M. I.; Miller, V. H.; Kayton, R. J.; Dixon, D. A.; Spencer, P. S. *Toxicol. Appl. Pharmacol.* **2001**, *177*, 121.

10.1021/ja0113394 CCC: $22.00

Scheme 2

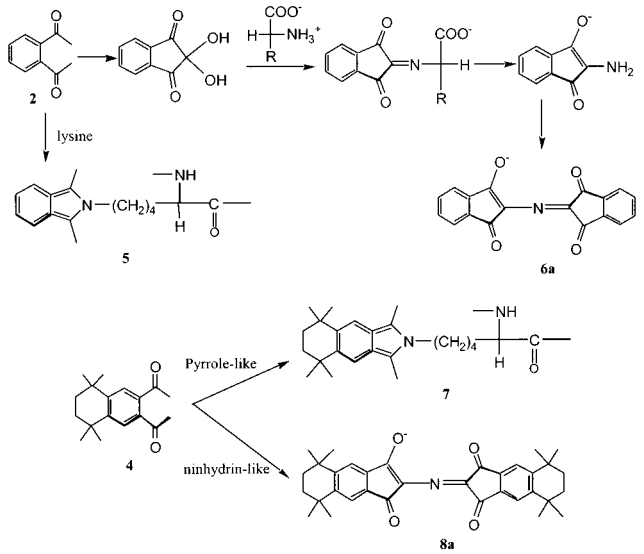

DAB or AETT develop blue discoloration of skin, eyes, and internal organs, including the brain and spinal cord.[3,4,5,8] On the basis of the available experimental data, it is believed that the chromogenic and neurotoxic properties of 1,2-DAB and 1,2-DATT are directly related through their reactions with amino acids.[3] Thus, knowledge about the mechanism of the chromogenic effects could provide valuable insights into the fundamental mechanism of the neurotoxicity. Mechanistic understanding of both chromogenic and neurotoxic effects could lead to the development of biomarkers of exposure to these neurotoxic compounds.

A variety of experimental studies have provided insights into the molecular mechanism of the chromogenic effects of 1,2-DAB (**2**) and 1,2-DATT (**4**). Based on available experimental results and structure−activity considerations, two possibilities have been suggested in the literature.[3] First, the chromogenicity is proposed to result from the formation of a ninhydrin-like compound that reacts with proteins to generate a colored pigment,[3] i.e., Ruhemann's purple, **6** or **8** (the chromophore), as shown in Scheme 2. For this to occur, the 1,2-diacetyl moiety of 1,2-DATT or 1,2-DAB would have to undergo an internal aldol condensation, followed by oxidation, loss of water, and further oxidation to yield a triketo structure representing an oxidized form of a ninhydrin-like compound.[3] The other hypothesis is that 1,2-DAB or 1,2-DATT reacts with the ϵ-amino groups of lysine in a manner equivalent to that of the neurotoxic aliphatic γ-diketones (such as 2,5-hexanedione, 2,5-HD, the active metabolite of the solvent *n*-hexane) that form 2,5-dimethylpyrrole adducts with proteins, including neurofilament peptides.[9] According to this hypothesis, the chromophores responsible for the chromogenic effects of 1,2-DAB and 1,2-DATT should be the pyrrole-like adducts **5** and **7** (Scheme 2). The former hypothesis is supported by well-established chemistry[10] of the ninhydrin color test leading to a blue color. The latter hypothesis is supported by the experimental demonstration that 1,2-DAB induces 2,5-HD-like giant axonal swellings filled with neurofilaments.[8] A very recent experimental study suggests that ninhydrin formation does not directly lead to neuropathological behavior[7] but cannot explicity rule out that ninhydrin is present as the chromophore due to varying in vivo diffusion and reaction processes.

There have been dramatic changes in computational chemistry over the past two decades. Electronic structure theory has become an effective and powerful tool for use in predicting the properties of a wide range of molecules including geometries, energetics, and spectroscopy (IR/Raman vibrational spectra, NMR, and UV−vis). One of the main reasons for the acceleration of the use of electronic structure theory in predicting molecular properties for larger molecules has been the development of density functional theory (DFT).[11−13] The combination of low computational cost with reasonable accuracy has led to the successful application of the DFT method to the prediction of a broad range of properties of molecules in the ground state.[14] In contrast to the case of ground states, time-dependent density functional theory (TD-DFT) for treating excited-state properties[15−17] has only recently been applied to molecules,[18,19] although the theory itself was first proposed more than 20 years ago. Recent work has shown that TD-DFT can be used to reliably predict not only the location of the UV−vis excitation but also the oscillator strength (intensity of the transition).[20,21] In addition, Adamo and Barone[22] have tested TD-DFT calculations in aqueous solution, although the calculated results indicate that the solvent shifts of the calculated excitation energies are very small.

We have used a variety of electronic structure methods to predict the structures, energetics, and spectra of potential chromophores in order to assign the structures responsible for the chromogenic effects of the reaction with amino acids of the monocyclic aromatic neurotoxicant 1,2-DAB (**2**) and the putative metabolite 1,2-DATT of the dicyclic neurotoxicant AETT (**4**). We have studied structures from both hypothetical pathways. Detailed comparison of the calculated results with available experiment provides useful insights into the molecular mechanism of the chromogenic effects.

Computational Details

Geometries of all species considered in this study were fully optimized by using gradient-corrected DFT with Becke's three-parameter hybrid exchange functional and the Lee−Yang−Parr correlation functional (B3LYP)[23] and with the 6-31G(d) basis set.[24] Analytical second derivative calculations, which yield the harmonic

(8) Kim, M. S.; Kayton, R.; Muñiz, J.; Austin, D. R.; Spencer, P. S.; Sabri, M. *Microsc. Microanal.* **1999**, *5* (Suppl. 2), 1218.
(9) DeCaprio, A. P. In *Experimental and Clinical Neurotoxicology*, 2nd ed.; Spencer, P. S., Schaumburg, H. H., Eds.; Oxford University Press: New York, 2000; p 633.
(10) Roberts, J. D.; Caserio, M. C. *Basic Principles of Organic Chemistry*; Benjamin: New York, 1965; p 708.
(11) Hohenberg, P.; Kohn, W. *Phys. Rev. B* **1964**, *136*, 864.
(12) Kohn, W.; Sham, L. J. *Phys. Rev. A* **1965**, *140*, 1133.
(13) Parr, R. G.; Yang W. *Density-Functional Theory of Atoms and Molecules*; Oxford University Press: Oxford, 1989.
(14) *Recent Advances in Density Functional Methods, Part 1*; Chong, D. P., Ed.; World Scientific: Singapore, 1995.
(15) Ando, T. Z. *Phys. B* **1977**, *26*, 263.
(16) Zangwill, A.; Soven, P. *Phys. Rev. A* **1980**, *21*, 1561.
(17) Runge, E.; Gross, E. K. U. *Phys. Rev. Lett.* **1984**, *52*, 997.
(18) Bauernschmitt, R.; Ahlrichs, R. *Chem. Phys. Lett.* **1996**, *256*, 454.
(19) Casida, M. E.; Jamorski, C.; Casida, K. C.; Salahub, D. R. *J. Chem. Phys.* **1998**, *108*, 4439.
(20) Matsuzawa, N. N.; Ishitani, A.; Dixon, D. A.; Uda, T. *J. Phys. Chem. A* **2001,** *105*, 4953.
(21) Casida, M. E.; Salahub, D. R. *J. Chem. Phys.* **2000**, *113*, 8918.
(22) Adamo, C.; Barone, V. *Chem. Phys. Lett.* **2000**, *330*, 152.
(23) (a) Becke, A. D. *J. Chem. Phys.* **1993**, *98*, 5648. (b) Lee, C.; Yang, W.; Parr, R. G. *Phys. Rev. B* **1988**, *37*, 785. (c) Stephens, P. J.; Devlin, F. J.; Chabalowski, C. F.; Frisch, M. J. *J. Phys. Chem.* **1994**, *98*, 11623.
(24) Hehre, W. J.; Radom, L.; Schleyer, P. v. R.; Pople, J. A. *Ab Initio Molecular Orbital Theory*; John Wiley & Sons: New York, 1987.

vibrational frequencies, were performed at the optimized geometries to ensure that the optimized geometries are minima on the potential energy hypersurface (all real frequencies). The geometries optimized at the B3LYP/6-31G(d) level were further refined at the B3LYP/6-31+G(d) level of theory. In addition, the 6-311G(d,p) basis set[24] was also tested in the geometry optimization on **5m**, a model compound of the pyrrole-like adduct **5,** to ensure that the double-ζ basis set used in geometry optimization is adequate. Geometries optimized at the B3LYP/6-31+G(d) level were used in the calculation of the energies of the singlet vertical excited states to evaluate the UV−vis spectrum by using both the single-excitation configuration interaction (CIS) method[25] using a Hartree−Fock (HF) reference function and the time-dependent DFT (TD-DFT) method[26] using the B3LYP functional. For two key species (**6a** and **6b**), we also carried out CAS(*n*,*m*)-MP2 calculations, i.e., a complete active space multiconfiguration self-consistent field (CASSCF) calculation including *n* electrons occupying *m* orbitals in the active space followed by second-order Møller−Plesset (MP2) perturbation on the multiconfigurational reference state.[27] The basis set dependence of the calculated excitation energies was studied for **5m**, **6a**, and **6b** with the following basis sets: 6-31+G(d), 6-311++G(d,p), and aug-cc-pVDZ.[28] In addition, larger basis sets, including 6-31++G(d,p), 6-311++G(2d,2p), 6-311++G(3df,3pd), and aug-cc-pVTZ,[28] were also used in some of the energy calculations (see below).

For the key molecules **6a** and **6b**, the geometries optimized at the B3LYP/6-31+G(d) level were used in self-consistent reaction field (SCRF) calculations at the HF/6-31+G(d) level in order to calculate the free energies of solvation in aqueous solution. The calculated free energy in solution was taken as the free energy calculated at various levels in the gas phase with the B3LYP/6-31+G(d) zero-point and other vibrational energy corrections plus the solvent shift calculated at the HF/6-31+G(d) level. The present SCRF method was developed and implemented recently in a local version of the *GAMESS* program[29] by one of us and is called the surface and volume polarizations for electrostatic interaction (SVPE) model.[30] The SVPE model is also known as the fully polarizable continuum model (FPCM)[31−33] because it fully accounts for both surface and volume polarization effects in the SCRF calculation through an efficient three-dimensional integration algorithm.[30a] Since the solute cavity surface is defined as a solute electron charge isodensity contour determined self-consistently during the SVPE iteration process, the SVPE results, converged to the exact solution of Poisson's equation with a given numerical tolerance, depend only on the contour value at a given dielectric constant and a certain quantum chemical calculation level.[30a] This single-parameter value has been determined to be 0.001 au on the basis of an extensive calibration study.[30b] The SVPE procedure using the 0.001 au contour has been shown to be reliable for predicting the free energy of solvation and the pK_a in other biologically interesting systems.[30−33] To estimate the solvent effects on the geometries of **6a** and **6b**, we also performed geometry optimizations by using the quantum Onsager model as implemented in the *Gaussian98* program.[34] The cavity radii used for these calculations on **6a** and **6b** were determined as 8.042480 and 8.108927 Å, respectively, by using the standard procedure[35] of the largest distance between the center of mass and the most distant atom plus the van der Waals radius of the atom (i.e., 1.2 Å for H atom). The dielectric constant of water used for the solvation calculations is 78.5.

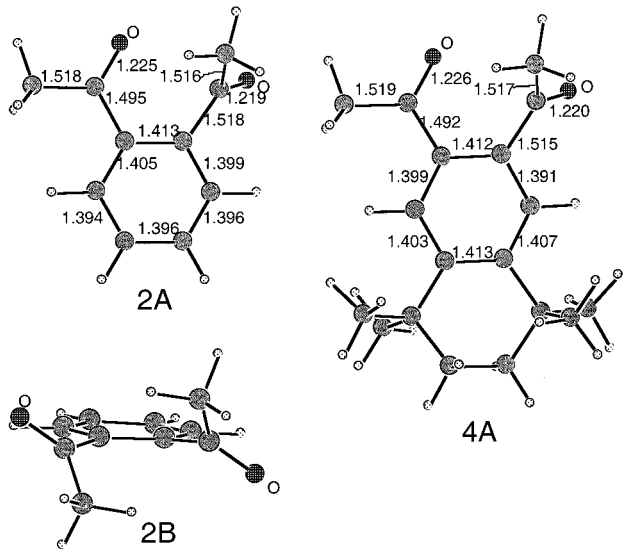

Figure 1. Geometries of 1,2-DAB (**2**) and 1,2-DATT (**4**) optimized at the B3LYP/6-31+G(d) level. The unlabeled atoms are C (larger balls) or H (smaller balls). Key bond lengths are given in angstroms.

Geometry optimizations and ground-state energy evaluations were performed by using the *Gaussian98*[34] and *NWChem* programs.[36] The *Gaussian98* program was used to carry out the CIS, TD-DFT, CAS-MP2, and quantum Onsager calculations. A local version[30a] of the *GAMESS* program[29] was used to perform the SVPE calculations. All calculations were performed on a 16-processor SGI Origin 2000 and a 512-processor IBM SP supercomputer.

Results and Discussion

Optimized Geometries. The optimized geometries for 1,2-DAB (**2**) and 1,2-DATT (**4**) are shown in Figure 1. As shown in Figure 1, we found two stable structures for 1,2-DAB (**2**), with **2A** the most stable. The energy of **2B** is calculated to be ∼2 kcal/mol higher than that of **2A** at the B3LYP/6-31+G(d)//B3LYP/6-31+G(d) and also at the MP2/aug-cc-pVDZ//B3LYP/6-31+G* levels. Similarly, we found two stable conformers for DATT (**4**). The most stable structure of 1,2-DATT (**4**) is **4A**,

(25) Foresman, J. B.; Head-Gordon, M.; Pople, J. A.; Frisch, M. J. *J. Phys. Chem.* **1992**, *96*, 135.
(26) Stratmann, R. E.; Scuseria, G. E.; Frisch, M. J. *J. Chem. Phys.* **1998**, *109*, 8218.
(27) McDouall, J. J.; Peasley, K.; Robb, M. A. *Chem. Phys. Lett.* **1988**, *148*, 183.
(28) Kendall, R. A.; Dunning, T. H., Jr.; Harrison, R. J. *J. Chem. Phys.* **1992**, *96*, 6796.
(29) Schmidt, M. W.; Baldridge, K. K.; Boatz, J. A.; Elbert, S. T.; Gordon, M. S.; Jensen, J. H.; Koseki, S.; Matsunaga, N.; Nguyen, K. A.; Su, S. J.; Windus, T. L.; Dupuis, M.; Montgomery, J. A. *J. Comput. Chem.* **1993**, *14*, 1347.
(30) (a) Zhan, C.-G.; Bentley, J.; Chipman, D. M. *J. Chem. Phys.* **1998**, *108*, 177. (b) Zhan, C.-G.; Chipman, D. M. *J. Chem. Phys.* **1998**, *109*, 10543. (c) Zhan, C.-G.; Chipman, D. M. *J. Chem. Phys.* **1999**, *110*, 1611. (d) Zhan, C.-G.; Landry, D. W.; Ornstein, R. L. *J. Phys. Chem. A* **2000**, *104*, 7672.
(31) (a) Zhan, C.-G.; Norberto de Souza, O.; Rittenhouse, R.; Ornstein, R. L. *J. Am. Chem. Soc.* **1999**, *121*, 7279. (b) Zhan, C.-G.; Niu, S.; Ornstein, R. L. *J. Chem. Soc., Perkin Trans. 2* **2001**, 23. (c) Zhan, C.-G.; Zheng, F. *J. Am. Chem. Soc.* **2001**, *123*, 2835.
(32) Zhan, C.-G.; Landry, D. W.; Ornstein, R. L. *J. Am. Chem. Soc.* **2000**, *122*, 2621.
(33) Zhan, C.-G.; Landry, D. W. *J. Phys. Chem. A* **2001**, *105*, 1296.
(34) Frisch, M. J.; Trucks, G. W.; Schlegel, H. B.; Scuseria, G. E.; Robb, M. A.; Cheeseman, J. R.; Zakrzewski, V. G.; Montgomery, J. A.; Stratmann, R. E.; Burant, J. C.; Dapprich, S.; Millam, J. M.; Daniels, A. D.; Kudin, K. N.; Strain, M. C.; Farkas, O.; Tomasi, J.; Barone, V.; Cossi, M.; Cammi, R.; Mennucci, B.; Pomelli, C.; Adamo, C.; Clifford, S.; Ochterski, J.; Petersson, G. A.; Ayala, P. Y.; Cui, Q.; Morokuma, K.; Malick, D. K.; Rabuck, A. D.; Raghavachari, K.; Foresman, J. B.; Cioslowski, J.; Ortiz, J. V.; Stefanov, B. B.; Liu, G.; Liashenko, A.; Piskorz, P.; Komaromi, I.; Gomperts, R.; Martin, R. L.; Fox, D. J.; Keith, T.; Al-Laham, M. A.; Peng, C. Y.; Nanayakkara, A.; Gonzalez, C.; Challacombe, M.; Gill, P. M. W.; Johnson, B.; Chen, W.; Wong, M. W.; Andres, J. L.; Gonzalez, A. C.; Head-Gordon, M.; Replogle, E. S.; Pople, J. A. *Gaussian 98*, Revision A.6; Gaussian, Inc.: Pittsburgh, PA, 1998.
(35) Christiansen, O.; Mikkelsen, K. *J. Chem. Phys.* **1999**, *110*, 8348.
(36) Anchell, J.; Apra, E.; Bernholdt, D.; Borowski, P.; Bylaska, E.; Clark, T.; Clerc, D.; Dachsel, H.; de Jong, W. A.; Deegan, M.; Dupuis, M.; Dyall, K.; Elwood, D.; Fann, G.; Fruchtl, H.; Glendenning, E.; Gutowski, M.; Harrison, R.; Hess, A.; Jaffe, J.; Johnson, B.; Ju, J.; Kendall, R.; Kobayashi, R.; Kutteh, R.; Lin, Z.; Littlefield, R.; Long, X.; Meng, B.; Nichols, J.; Nieplocha, J.; Rendall, A.; Rosing, M.; Sandrone, G.; Stave, M.; Straatsma, T.; Taylor, H.; Thomas, G.; van Lenthe, J.; Windus, T.; Wolinski, K.; Wong, A.; Zhang, Z. *NWChem*, Version 4.0; Pacific Northwest National Laboratory: Richland, WA, 1999.

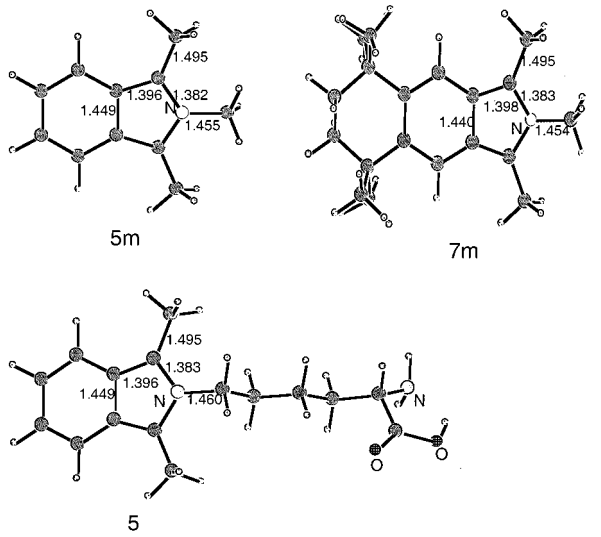

Figure 2. Geometries of the pyrrole-like reaction products **5**, **5m**, and **7m** optimized at the B3LYP/6-31+G(d) level. The unlabeled atoms are C (larger balls) or H (smaller balls). Key bond lengths are given in angstroms.

as shown in Figure 1; the other stable conformer of **4** similar to **2B** is ∼3 kcal/mol higher in energy than **4A**.

The stable geometries optimized for the model compounds **5m** and **7m** of the possible pyrrole-like adducts (**5** and **7**) formed from 1,2-DAB (**2**) and 1,2-DATT (**4**) are shown in Figure 2. The structures of **5m** and **7m** appear to be flexible in terms of rotation of the methyl groups. However, we found only one conformer (shown in Figure 2) associated with a local minimum on the corresponding potential energy surface for each of the two compounds. The other possible conformers tested were found to be associated with saddle points. In **5m** and **7m**, we retain only one C atom from the protein (or amino acid) in the model pyrrole-like adduct, and we add hydrogen atoms to this C atom bonding to the N atom to complete its valency. It is expected that this simplification will not considerably affect the first excitation energy of **5** and **7**, as discussed below. For verification, we also optimized a stable geometry of **5** with the entire lysine structure, as shown in Scheme 2 and Figure 2.

For the ninhydrin-like reaction products **6** and **8**, the structures of the deprotonated states, **6a** and **8a** (anions), could be either planar or nonplanar. The nonplanar structure is defined such that the two equivalent parts of the structure centered at the N atom do not share the same plane. Our calculated results reveal that the planar structure of **6a** with C_{2v} symmetry, denoted by **6a-P** in Figure 3, is a transition state (first-order saddle point) connecting two equivalent nonplanar structures with C_2 symmetry (local minimum). The energy barrier calculated at the B3LYP/6-31+G* level is ∼5 kcal/mol, and, thus, only the nonplanar C_2 structure of **6a** (Figure 3) is associated with a local minimum, as is the nonplanar C_2 structure of **8a** (Figure 4.) In addition to the deprotonated structures, **6a** and **8a**, we also considered the neutral protonated states. The protonation of **6a** could occur at either an O atom (**6b′**) or a N atom (**6b**) (Scheme 3). Protonation at the N atom produces a stable nonplanar structure, **6b**, with C_2 symmetry and a transition state, **6b-P**, corresponding to a planar structure with C_{2v} symmetry connecting two equivalent stable **6b** structures. (See Figure 5 for the optimized geometries.) The energy barrier connecting the two stable C_2 structures of **6b** is calculated at the B3LYP/6-31+G* level to be ∼3 kcal/mol. The four O atoms in **6a** exist

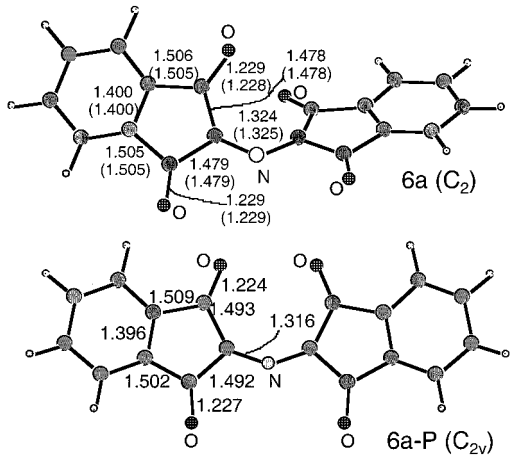

Figure 3. Deprotonated state of product formed from the ninhydrin-like reaction of **2**: geometries of stable structure (**6a**) and transition state (**6a-P**) optimized at the B3LYP/6-31+G(d) level. The unlabeled atoms are C (larger balls) or H (smaller balls). Key bond lengths are given in angstroms. The values given in parentheses are the corresponding geometric parameters optimized in aqueous solution using the quantum Onsager model at the B3LYP/6-31+G(d) level.

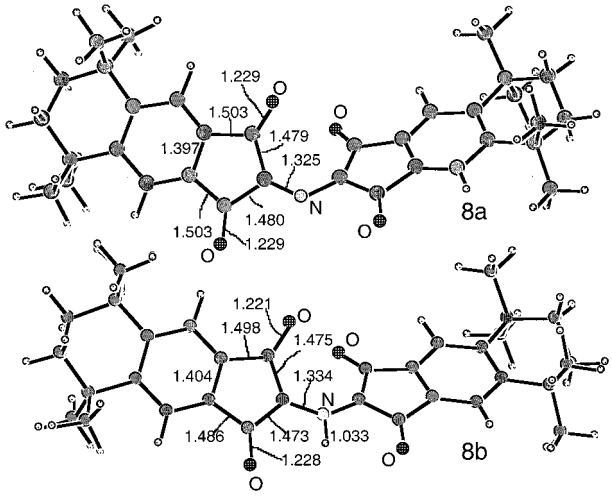

Figure 4. Geometries of the most stable deprotonated and protonated structures (**8a** and **8b**) of product formed from the ninhydrin-like reaction of **4** optimized at the B3LYP/6-31+G(d) level. The unlabeled atoms are C (larger balls) or H (smaller balls). Key bond lengths are given in angstroms.

in two different chemical environments; thus, a proton could attach to two different kinds of O atoms, producing **6b′-Oa** and **6b′-Ob**. The optimizations of **6b′-Oa** and **6b′-Ob** geometries started from nonplanar structures based on **6a**. As shown in Figure 5, the converged geometry of **6b′-Oa** is planar, whereas that of **6b′-Ob** is nonplanar; both are minima on the potential energy surface. Thus, we obtained a total of three stable structures for the protonated state and found that a proton attached to the N atom instead of an O atom is the most stable protonated structure, **6b**. The structures, **6b′-Oa** and **6b′-Ob**, with the proton bonded to an O atom are 5.3 and 9.9 kcal/mol higher in energy, respectively, at the B3LYP/6-31+G* level. The lowest energy protonated O atom structure, **6b′-Oa**, has a hydrogen bond between the OH on one ring and the carbonyl on the adjacent ring, and in the higher energy structure, **6b′-Ob**, there is no hydrogen bond. Similarly, one can expect the most stable structure of protonated state, **8b**, to be associated with the protonation at the N atom (Scheme 3). The optimized geometry of **8b** is depicted in Figure 4.

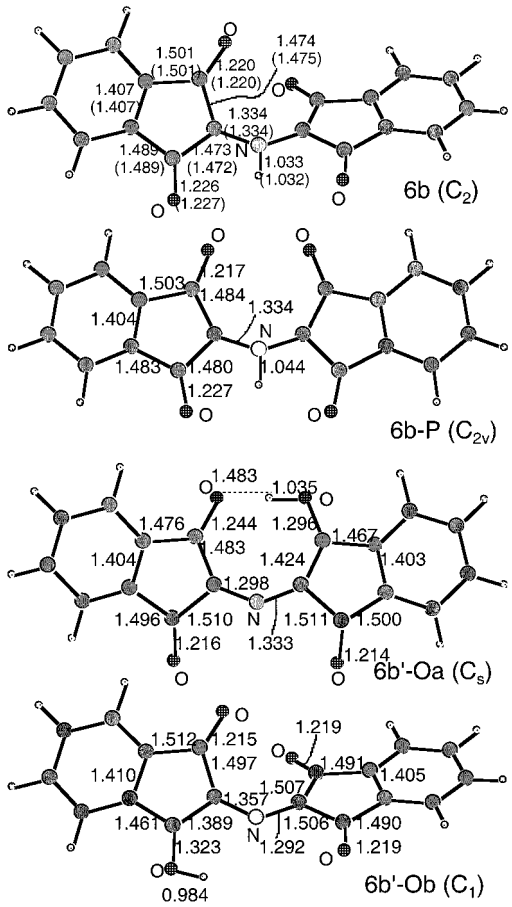

Figure 5. Protonated states of product formed from the ninhydrin-like reaction of **2**: geometries of stable structures (**6b**, **6b′-Oa**, and **6b′-Ob)** and transition state (**6b-P)** optimized at the B3LYP/6-31+G(d) level. The unlabeled atoms are C (larger balls) or H (smaller balls). Key bond lengths are given in angstroms. The values given in parentheses are the corresponding geometric parameters optimized in aqueous solution using the quantum Onsager model at the B3LYP/6-31+G(d) level.

Scheme 3

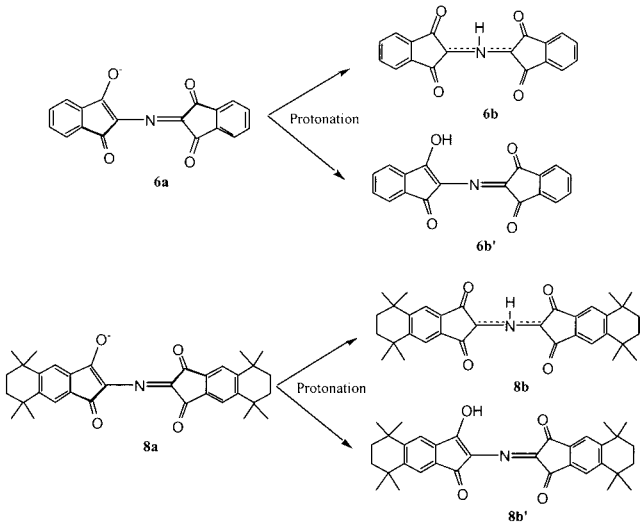

To calculate the thermodynamic equilibration between the deprotonated and protonated states, we determined the pK_a for the deprotonation process **6b** → **6a** + H^+ by performing a series of first-principles calculations on the gas-phase geometries of **6a** and **6b**, using the DFT and MP2 methods with various basis sets for the gas-phase electronic energy difference and the SVPE/HF/6-31+G(d) method for the solvation energy difference. The value of the SVPE/HF/6-31+G(d) free energy difference for **6a** and **6b** is −40.6 kcal/mol. We also optimized geometries of **6a** and **6b** in solution using the quantum Onsager model implemented in the *Gaussian98* program. As shown in Figures 3 and 5, the differences between the geometric parameters optimized in solution and those in gas phase are negligible; the largest difference in bond length is ∼0.001 Å. As a result, the change from the free energy difference estimated by using the gas-phase geometries to that estimated by using the solution geometries is negligible (<0.1 kcal/mol). It is also necessary for the prediction of the absolute pK_a to know the absolute free energy of the proton in aqueous solution. For the gas-phase proton, accounting for contributions of proton translation to enthalpy and entropy, we have $H(T = 298\ \text{K}) = 1.5$ kcal/mol and $-TS = -7.8$ kcal/mol at $T = 298$ K.[37] The "experimental" hydration free energy of the proton has a wide range (from −252.6 to −264.1 kcal/mol).[38] The largest negative value, −264.1 kcal/mol, is the most recent[39a] and is close to recent theoretical values.[38,40] We recently calculated[40] the absolute hydration free energy of the proton, $\Delta G^{298}_{\text{hyd}}(H^+)$, by using a high-level, ab initio method of incorporating a hybrid supermolecule continuum approach based on the same SVPE procedure[30] used in the present study. $\Delta G^{298}_{\text{hyd}}(H^+)$ was accurately predicted to be −262.4 kcal/mol. Although it has not been possible to isolate one type of ion and measure its absolute hydration free energy by experiment, direct experimental thermodynamic data for different pairs of ions can lead to relative magnitudes of the ionic hydration free energies. The high accuracy of the predicted absolute hydration free energy of the proton has been confirmed by applying the same computational protocol to predict the absolute hydration free energy of Li^+: $\Delta G^{298}_{\text{hyd}}(Li^+) = -125.1$ kcal/mol, which is larger than $\Delta G^{298}_{\text{hyd}}(H^+)$ by 137.3 kcal/mol.[40] The calculated hydration free energy change for solvation of a proton to solvation of Li^+ is 137.5 kcal/mol from the latest collection of experimental data[39a] and 137.0 kcal/mol from the earlier experimental data.[39b] Our theoretical value is between the two experimental values. Thus, the total free energy of solvation for the deprotonation process is calculated to be −303.0 kcal/mol. The pK_a is calculated as $\text{p}K_a = \Delta G_{\text{sol}}/(2.303RT)$ at $T = 298$ K. The calculated pK_a results as a function of electronic structure method are summarized in Table 1. We first note that **6b** is a strong gas-phase acid with a gas-phase acidity comparable to that of H_2SO_4, which has a value of 312.2 kcal/mol[41] calculated at the G2 level.[42] There is a significant difference between the B3LYP/6-31+G(d) result and the B3LYP/6-31++G(d,p) result; similar differences have been noted in previously reported studies.[43] Results using the B3LYP functional and even larger basis sets are not significantly different from the B3LYP/6-31++G(d,p) result, indicating that

(37) Chase, M. W., Jr., NIST-JANAF Tables (4th ed.). *J. Phys. Chem. Ref. Data* **1998**, *Suppl. 1*, Mono. 9.
(38) Tawa, G. J.; Topol, I. A.; Burt, S. K.; Caldwell, R. A.; Rashin, A. A. *J. Chem. Phys.* **1998**, *109*, 4852.
(39) (a) Tissandier, M. D.; Cowen, K. A.; Feng, W. Y.; Gundlach, E.; Cohen, M. H.; Earhart, A. D.; Coe, J. V. *J. Phys. Chem. A* **1998**, *102*, 7787. (b) Friedman, H. L.; Krishnan, V. V. *Water: A comprehensive treatise*; Plenum: New York, 1973.
(40) Zhan, C.-G.; Dixon, D. A. *J. Phys. Chem. A* **2001**, *105*, 11534.
(41) Rustad, J. R.; Dixon, D. A.; Kubicki, J. D.; Felmy, A. R. *J. Phys. Chem. A* **2000**, *104*, 4051.
(42) Curtiss, L. A.; Raghavachari, K.; Trucks, G. W.; Pople J. A. *J. Chem. Phys.* **1991,** *94*, 7221.

Table 1. Free Energy Change (in kcal/mol, at 298 K) for **6b** → **6a** + H^+ and the Corresponding pK_a Determined by Performing Single-Point Energy Calculations with Geometries Optimized at the B3LYP/6-31+G(d) Level

energy calculation	ΔG_{gas}	ΔG_{sol}	pK_a
B3LYP/6-31+G(d)	306.8	3.8	2.8
B3LYP/6-31++G(d,p)	308.7	5.8	4.3
B3LYP/6-311++G(d,p)	308.3	5.4	4.0
B3LYP/6-311++G(2d,2p)	309.0	6.1	4.5
B3LYP/6-311++G(3df,3pd)	309.2	6.2	4.5
MP2/6-31++G(d,p)	312.7	9.7	7.1
MP2/aug-cc-pVDZ	309.7	6.8	5.0
MP2/aug-cc-pVTZ	311.2	8.3	6.1

the 6-31++G(d,p) basis set is adequate for the pK_a prediction at the B3LYP level. We performed a higher level energy calculation at the second-order Møller−Plesset (MP2) level with the 6-31++G(d,p), aug-cc-pVDZ, and aug-cc-pVTZ basis sets. The MP2 results are more sensitive to the basis set. Our best estimate of the pK_a value, calculated at the MP2/aug-cc-pVTZ level, is about 6. A value of p$K_a \approx 6$ indicates that when the pH value is about 6, the concentrations of the deprotonated and protonated structures should be equal to each other. At lower pH, the protonated structure should be dominant, whereas at higher pH the deprotonated structure should be dominant. Particularly, about 10% of **6** is protonated at pH = 7 for a neutral solution. It should be pointed out that we cannot exclude the possibility of the basis-set-converged DFT result (p$K_a \approx 5$) being actually more reliable than the MP2 result (p$K_a \approx 6$). Nevertheless, all of the DFT and MP2 results lead to the same qualitative conclusion that the pK_a of **6** should be smaller than 7 and, therefore, in either case the deprotonated structure should be dominant in a neutral aqueous solution.

Electronic Excitation Energies. Based on the optimized geometries of the most stable structures depicted in Figures 1−3, we calculated the electronic excitation energies at various levels of theory. The first excitation energies calculated at the geometries optimized at the B3LYP/6-31+G(d) level are summarized in Table 2. For **5m**, the TD-DFT/B3LYP/6-31+G(d)//B3LYP/6-311G(d,p) result, 3.59 eV (∼345 nm), is nearly identical to the TD-DFT/B3LYP/6-31+G(d)//B3LYP/6-31+G(d) result, 3.57 eV (∼347 nm). The appropriateness of the models **5m** and **7m** of the pyrrole-like adducts **5** and **7** can be assessed by a comparison of the results calculated for both **5m** and **5** using the same protocol, TD-DFT at the B3LYP/6-31+G* level. The first excitation energy, 3.57 eV (347 nm), calculated for **5m** is only 0.14 eV larger than that, 3.43 eV (361 nm), calculated for **5**, indicating that models **5m** and **7m** are adequate.

As shown in Table 2, the calculated excitation energies are not sensitive to the basis set used in the calculations. For the calculations using the same method (CIS or TD-DFT), the largest difference between the results calculated with the 6-31+G(d) basis set and with the 6-311++G(d,p) basis set is 0.07 eV. The largest difference between the results calculated with the 6-311++G(d,p) basis set and with the aug-cc-pVDZ basis set is 0.02 eV. Thus, the computationally efficient 6-31+G(d) basis set is adequate for this study, and we performed calculations on all of the structures with the 6-31+G(d) basis set. For the two most important molecules, **6a** and **6b**, we also performed more sophisticated CAS-MP2 calculations, in addition to the CIS and TD-DFT calculations. The CAS(2,2)-MP2 results are close to the corresponding TD-DFT results. The reliability of the CAS(2,2)-MP2 calculations was further examined by performing CAS(4,4)-MP2 calculations on the key species **6a**. The active space in the CAS(2,2)-MP2 calculations includes only one a orbital (HOMO) and one b orbital (LUMO). The active space in the CAS(4,4)-MP2 calculations includes one more a orbital and one more b orbital, in addition to the HOMO and LUMO. The first excitation energy of **6a**, 2.01 eV, calculated at the CAS(4,4)-MP2 level is only ∼0.11 eV higher than the corresponding CAS(2,2)-MP2 result, 1.90 eV (∼651 nm), and is nearly identical to the TD-DFT result, 2.00 eV (∼618 nm). The agreement between the TD-DFT results and the CAS-MP2 results reveals that the TD-DFT method is reliable for the molecules considered in this study.

The excitation energies calculated using the CIS method are systematically larger than the corresponding TD-DFT results. Previous CIS calculations[20,25,44] in comparison with experimental data indicate that the CIS method systematically overestimates the excitation energies. This is not surprising, because the CIS method has been shown to do very well for vertical excitation energies in nonpolar molecules[25,45,46] but not nearly as well for carbonyl compounds due to the poor HF description of the polar C=O groups and the corresponding n→π^* and π→π^* states.[47] A recent study[20] on the electronic excitations of formaldehyde, a small carbonyl compound, demonstrated an excellent linear correlation between the 18 available experimental values and the corresponding CIS results of the excitation energies:

$$E_{expt} = 1.02E_{calc} - 1.00 \text{ (eV)} \quad (1)$$

with a correlation coefficient of 0.967. This linear correlation was employed, in the present study, to correct all of the CIS results. Both the uncorrected (E_{calc}) and corrected ($1.02E_{calc} - 1.00$) results are given in Table 2. The empirically corrected CIS results are in quite good agreement with the corresponding TD-DFT results. This suggests that the TD-DFT results should provide reliable estimates of the excitation energies.

To further benchmark the methods used in this study, we performed CIS, TD-DFT, and CAS(2,2)-MP2 calculations on ethylene with the geometry optimized at the B3LYP/6-31+G(d) level. The values of the first excitation energy calculated at the CIS/6-31+G(d), TD-DFT/B3LYP/6-31+G(d), and CAS(2,2)-MP2/6-31+G(d) levels are 7.83 eV (158 nm), 7.18 eV (173 nm), and 6.98 eV (178 nm), respectively, and the corrected CIS result is 6.99 eV (177 nm). Compared to the experimental value of 7.15 eV (173 nm),[48] TD-DFT overestimates the first excitation energy by ∼0.03 eV (underestimating the wavelength by less than 1 nm). The corrected CIS and CAS(2,2)-MP2/6-31+G(d) results underestimate the first excitation energy by less than 0.2 eV (overestimating the wavelength by ∼4−5 nm). These values are certainly adequate for this study, and the TD-DFT result is surprisingly good, considering the moderate

(43) (a) Wiberg, K. B.; Castejon, H.; Keith, T. A. *J. Comput. Chem.* **1996**, *17*, 185. (b) Merrill, G. N.; Kass, S. R. *J. Phys. Chem.* **1996**, *100*, 17465.

(44) Foresman, J. B.; Frisch, Æ. *Exploring Chemistry with Electronic Structure Methods*, 2nd ed; Gaussian, Inc.: Pittsburgh, PA, 1996; p 216.

(45) Wiberg, K. B.; Hadad, C. M.; Foresman, J. B.; Chupka, W. A. *J. Phys. Chem.* **1992**, *96*, 10756.

(46) Wiberg, K. B.; Hadad, C. M.; Ellison, G. B.; Foresman, J. B. *J. Phys. Chem.* **1993**, *97*, 13586.

(47) Hadad, C. M.; Foresman, J. B.; Wiberg, K. B. *J. Phys. Chem.* **1993**, *97*, 4293.

(48) Merer, A. J.; Mulliken, R. S. *Chem. Rev.* **1969**, *69*, 639.

Table 2. First Electronic Excitation Energies (in eV) Calculated for 1,2-DAB, 1,2-DATT, and Their Possible Products [Corresponding Wavelengths (in nm) of the Absorption Are Given in Parentheses][a]

	1,2-DAB and possible products				1,2-DATT and possible products			
calculation method	**2**	**5m**	**6a**	**6b**	**4**	**7m**	**8a**	**8b**
CIS/6-31+G(d)	4.95 (250)	4.40 (282)	2.95 (420)	3.38 (367)	4.98 (249)	4.32 (287)	2.92 (425)	3.31 (375)
CIS/6-311++G(d,p)			2.92 (424)	3.33 (372)				
CIS/6-31+G(d) with correction[b]		3.48 (356)	2.01 (617)	2.45 (506)	4.08 (304)	3.41 (364)	1.98 (626)	2.38 (521)
CIS/6-311++G(d,p) with correction[b]			1.98 (626)	2.40 (517)				
TD-DFT/6-31+G(d)	3.68 (337)	3.57 (347)[c]	2.00 (618)	2.49 (498)	3.72 (333)	3.48 (356)	1.97 (629)	2.49 (497)
TD-DFT/6-311++G(d,p)		3.50 (354)						
TD-DFT/aug-cc-pVDZ		3.48 (356)						
CAS(2,2)-MP2/6-31+G(d)			1.90 (651)	2.41 (515)				
CAS(4,4)-MP2/6-31+G(d)			2.01 (616)					

[a] All calculations were performed with geometries optimized at the B3LYP/6-31+G(d) level. [b] An empirical correction, $1.02E_{calc} - 1.00$ (eV), was used to obtain these CIS results. [c] The corresponding result calculated for compound **5** is 3.43 eV (361 nm).

Table 3. Wavelengths λ (nm) and Oscillator Strengths f Calculated at the B3LYP/6-31+G(d) Level by Using the TD-DFT Method for the First 15 Electronic Excitations of 1,2-DAB and the Possible Products[a]

2		**5m**		**6a**		**6b**	
λ	f	λ	f	λ	f	λ	f
337	0.0032	347	0.0882	618	0.1931	498	0.0002
$(n_{CO} \rightarrow \pi^*_{CO} + \pi^*_{C6})$		$(\pi \rightarrow \pi^*)$		$(n_N + n_{CO} \rightarrow \pi^*_{C5} + \pi^*_{C6})$		$(n_{CO} \rightarrow \pi^*_{C5})$	
326	0.0035	327	0.0014	526	0.0104	480	0.0582
$(n_{CO} \rightarrow \pi^*_{CO} + \pi^*_{C6})$		$(\pi \rightarrow \sigma^*_{CH}\text{-R})$		$(n_N + n_{CO} \rightarrow \pi^*_{C5} + \pi^*_{C6})$		$(n_{CO} \rightarrow \pi^*_{C5})$	
278	0.0001	288	0.0058	519	0.0061	422	0.8246
$(n_{CO} \rightarrow \pi^*_{C6} + \pi^*_{CO})$		$(\pi \rightarrow \sigma^*_{CH}\text{-R})$		$(n_N + n_{CO} \rightarrow \pi^*_{C5} + \pi^*_{C6})$		$(\pi_{C5} \rightarrow \pi^*_{C5})$	
266	0.0273	277	0.0000	424	0.0001	396	0.0011
$(\pi_{C6} + n_{CO} \rightarrow \pi^*_{CO} + \pi^*_{C6})$		$(\pi \rightarrow \sigma^*_{CH}\text{-R})$		$(n_{CO} \rightarrow \pi^*_{C5} + \pi^*_{C6})$		$(n_{CO} \rightarrow \pi^*_{C5})$	
247	0.1265	263	0.0042	406	0.2704	381	0.0065
$(\pi_{C6} + n_{CO} \rightarrow \pi^*_{CO} + \pi^*_{C6})$		$(\pi \rightarrow \pi^*)$		$(n_{CO} \rightarrow \pi^*_{C5} + \pi^*_{C6})$		$(\pi_{C5} \rightarrow \pi^*_{C5})$	
239	0.0081	253	0.0003	400	0.0025	377	0.0614
$(n_{CO} \rightarrow \pi^*_{CO})$		$(\pi \rightarrow \pi^*_{CH}\text{-R})$		$(n_{CO} \rightarrow \pi^*_{C5} + \pi^*_{C6})$		$(n_{CO} \rightarrow \pi^*_{C5})$	
225	0.0646	253	0.0000	393	0.2378	371	0.0345
$(n_{CO} \rightarrow \pi^*_{C6})$		$(\pi \rightarrow \sigma^*_{CH}\text{-R})$		$(n_{CO} \rightarrow \pi^*_{C5} + \pi^*_{C6})$		$(\pi_{C5} \rightarrow \pi^*_{C5})$	
209	0.1761	251	0.0012	352	0.0082	355	0.0006
$(\pi_{C6} + n_{CO} \rightarrow \pi^*_{C6})$		$(\pi \rightarrow \sigma^*_{CH}\text{-R})$		$(n_N + n_{CO} \rightarrow \pi^*_{C6})$		$(\pi_{C6} + n_{CO} \rightarrow \pi^*_{C5})$	
205	0.0606	246	0.0027	344	0.0000	351	0.0108
$(\pi_{C6} + n_{CO} \rightarrow \pi^*_{C6} + \pi^*_{CO})$		$(\pi \rightarrow \sigma^*_{CN} + \sigma^*_{CH}\text{-R})$		$(n_{CO} \rightarrow \pi^*_{C5} + \pi^*_{C6})$		$(\pi_{C6} \rightarrow \pi^*_{C5})$	
204	0.0110	233	0.0686	342	0.0361	343	0.0076
$(n_{CO} \rightarrow \sigma^*_{CH}\text{-R})$		$(\pi \rightarrow \pi^*)$		$(n_{CO} \rightarrow \pi^*_{C5} + \pi^*_{C6})$		$(\pi_{C6} + n_{CO} \rightarrow \pi^*_{C5})$	
202	0.0815	230	0.0080	328	0.0038	340	0.0155
$(n_{CO} \rightarrow \pi^*_{CO})$		$(\pi \rightarrow \sigma^*_{CH}\text{-R})$		$(n_{CO} \rightarrow \pi^*_{C5} + \pi^*_{C6})$		$(n_{CO} \rightarrow \pi^*_{C5})$	
194	0.0105	224	0.0917	326	0.0462	340	0.0056
$(\pi_{C6} + n_{CO} \rightarrow \pi^*_{CO})$		$(\pi \rightarrow \sigma^*_{CH}\text{-R})$		$(n_{CO} \rightarrow \pi^*_{C5} + \pi^*_{C6})$		$(n_{CO} \rightarrow \pi^*_{C5})$	
192	0.0144	222	0.0000	319	0.0007	333	0.0004
$(n_{CO} \rightarrow \sigma^*_{CH}\text{-R})$		$(\pi \rightarrow \sigma^*_{CH}\text{-R})$		$(n_N + n_{CO} \rightarrow \sigma^*_{CH}\text{-R})$		$(\pi_{C6} + n_{CO} \rightarrow \pi^*_{C5})$	
191	0.0332	221	0.0578	318	0.0004	300	0.0004
$(n_{CO} \rightarrow \sigma^*_{CH}\text{-R})$		$(\pi \rightarrow \sigma^*_{CH}\text{-R})$		$(n_N + n_{CO} \rightarrow \sigma^*_{CH}\text{-R})$		$(n_{CO} \rightarrow \pi^*_{C5})$	
191	0.0019	213	0.0287	313	0.0001	300	0.0024
$(n_{CO} \rightarrow \pi^*_{CO} + \pi^*_{C6})$		$(\pi \rightarrow \sigma^*_{CH}\text{-R})$		$(n_{CO} \rightarrow \pi^*_{C5} + \pi^*_{C6})$		$(n_{CO} \rightarrow \pi^*_{C5})$	

[a] The assignment is given in parantheses below each pair of λ and f values. n_{CO} represents a lone-pair of O on CO group(s). n_N represents a lone-pair of N. π_{C6} and π^*_{C6} refer to the bonding and antibonding π on the benzene ring(s), respectively. π_{C5} and π^*_{C5} refer to the bonding and antibonding π on the five-membered ring(s), respectively. π^*_{CO} refers to antibonding π on CO. π and π^* without a subscript represent the bonding and antibonding π on the whole conjugated π system in **5m**. σ^*_{CH} and σ^*_{CN} represent the antibonding σ on C−H and C−N bonds, respectively. R indicates that the excited state has Rydberg character.

(although nontrivial) computational cost. These benchmarks indicate that theoretical predictions based on both the CAS-MP2 and TD-DFT calculations are reliable. The CIS calculations, together with the empirical correction of systematic deviation, can also lead to reasonable predictions.

It is not surprising, as shown in Tables 3 and 4, that the predicted wavelengths and oscillator strengths for the first 15 excitations of **7m** are very similar to those of **5m**, considering the similarity in the structures. The predicted wavelengths and oscillator strengths for the first 15 excitations of **8a** and **8b** are also similar to those of **6a** and **6b**, respectively. Thus, the UV−vis spectra of the potential chromophores starting from 1,2-DAB and 1,2-DATT are very similar. The results summarized in Tables 2−4 clearly show that only the products of the ninhydrin-like reactions, i.e., **6** and **8**, have absorption in the visible region ($\lambda > \sim$400 nm and $\lambda < \sim$700 nm).[49] The other species under consideration here, i.e., **2**, **4**, **5**, and **7**, are colorless. These results suggest that the chromogenic effects of 1,2-DAB

Table 4. Wavelengths λ (nm) and Oscillator Strengths *f* Calculated Using the TD-DFT Method at the B3LYP/6-31+G(d) Level for the First 15 Electronic Excitations of 1,2-DATT and Possible Products[a]

4		**7m**		**8a**		**8b**	
λ	f	λ	*f*	λ	*f*	λ	*f*
333	0.0031	356	0.0684	629	0.2692	497	0.0002
($n_{CO} \rightarrow \pi^*_{CO}$)		($\pi \rightarrow \pi^*$)		($n_N + n_{CO} \rightarrow \pi^*_{C5} + \pi^*_{C6}$)		($n_{CO} \rightarrow \pi^*_{C5}$)	
325	0.0051	340	0.0000	513	0.0081	483	0.2181
($n_{CO} \rightarrow \pi^*_{CO}$)		($\pi \rightarrow \sigma^*_{CH}$-R)		($n_N + n_{CO} \rightarrow \pi^*_{C5} + \pi^*_{C6}$)		($n_{CO} \rightarrow \pi^*_{C5}$)	
282	0.0092	303	0.0051	507	0.0063	441	1.0376
($n_{CO} \rightarrow \pi^*_{C6} + \pi^*_{CO}$)		($\pi \rightarrow \sigma^*_{CH}$-R)		($n_N + n_{CO} \rightarrow \pi^*_{C5} + \pi^*_{C6}$)		($\pi_{C5} \rightarrow \pi^*_{C5}$)	
275	0.0269	298	0.0002	426	0.0001	398	0.0022
($\pi_{C6} + n_{CO} \rightarrow \pi^*_{CO} + \pi^*_{C6}$)		($\pi \rightarrow \sigma^*_{CH}$-R)		($n_{CO} \rightarrow \pi^*_{C5} + \pi^*_{C6}$)		($n_{CO} \rightarrow \pi^*_{C5}$)	
262	0.1906	274	0.0000	410	0.5540	386	0.0001
($\pi_{C6} + n_{CO} \rightarrow \pi^*_{CO}$)		($\pi \rightarrow \sigma^*_{CH}$-R)		($\pi_{C5} + n_{CO} \rightarrow \pi^*_{C5} + \pi^*_{C6}$)		($\pi_{C5} \rightarrow \pi^*_{C5}$)	
234	0.0013	273	0.0109	394	0.0015	381	0.0004
($n_{CO} \rightarrow \pi^*_{CO}$)		($\pi \rightarrow \pi^*$)		($\pi_{C5} + n_{CO} \rightarrow \pi^*_{C5}$)		($n_{CO} \rightarrow \pi^*_{C5}$)	
228	0.1453	272	0.0006	389	0.1204	376	0.0448
($\pi_{C6} + n_{CO} \rightarrow \pi^*_{C6} + \pi^*_{CO}$)		($\pi \rightarrow \sigma^*_{CH}$-R)		($\pi_{C5} + n_{CO} \rightarrow \pi^*_{C5} + \pi^*_{C6}$)		($n_{CO} \rightarrow \pi^*_{C5}$)	
222	0.2693	267	0.0004	373	0.0001	375	0.0080
($\pi_{C6} + n_{CO} \rightarrow \pi^*_{C6} + \pi^*_{CO}$)		($\pi \rightarrow \sigma^*_{CH}$-R)		($n_N + n_{CO} \rightarrow \sigma^*_{CH}$-R)		($n_{CO} \rightarrow \pi^*_{C5}$)	
216	0.0786	260	0.0000	373	0.0002	367	0.0108
($\pi_{C6} + n_{CO} \rightarrow \pi^*_{C6} + \pi^*_{CO}$)		($\pi \rightarrow \sigma^*_{CH} + \sigma^*_{CC}$-R)		($n_N + n_{CO} \rightarrow \sigma^*_{CH}$-R)		($\pi_{C5} \rightarrow \pi^*_{C5}$)	
212	0.0038	255	0.0014	356	0.0092	365	0.0289
($\sigma_{CC} + \sigma_{CH} \rightarrow \pi^*_{CO}$)		($\pi \rightarrow \pi^* + \sigma^*_{CH}$)		($n_N + n_{CO} \rightarrow \pi^*_{C6}$)		($\pi_{C5} \rightarrow \pi^*_{C5}$)	
212	0.0066	245	0.0033	342	0.0003	354	0.0261
($n_{CO} \rightarrow \sigma^*_{CH}$)		($\pi \rightarrow \sigma^*_{CH} + \sigma^*_{CN}$-R)		($n_{CO} \rightarrow \pi^*_{C5} + \pi^*_{C6}$)		($\pi_{C6} \rightarrow \pi^*_{C5}$)	
210	0.0070	243	0.0036	338	0.0554	338	0.0000
($\sigma_{CC} + \sigma_{CH} \rightarrow \pi^*_{CO}$)		($\pi \rightarrow \sigma^*_{CH}$-R)		($n_N + n_{CO} \rightarrow \pi^*_{C5} + \pi^*_{C6}$)		($n_{CO} \rightarrow \pi^*_{C5}$)	
203	0.0727	242	0.0042	332	0.0001	336	0.0114
($\pi_{C6} + n_{CO} \rightarrow \sigma^*_{CH}$)		($\pi \rightarrow \sigma^*_{CH}$-R)		($n_N + n_{CO} \rightarrow \sigma^*_{CH}$-R)		($n_{CO} \rightarrow \pi^*_{C5}$)	
203	0.0218	240	0.0014	331	0.0005	296	0.0001
($\pi_{C6} + n_{CO} \rightarrow \sigma^*_{CH}$)		($\pi \rightarrow \sigma^*_{CH}$-R)		($n_N + n_{CO} \rightarrow \sigma^*_{CH}$-R)		($n_{CO} \rightarrow \pi^*_{C5}$)	
200	0.0064	238	0.0697	326	0.0031	296	0.0016
($\pi_{C6} + n_{CO} \rightarrow \pi^*_{CO}$)		($\pi \rightarrow \pi^*$)		($n_{CO} \rightarrow \pi^*_{C5} + \pi^*_{C6}$)		($n_{CO} \rightarrow \pi^*_{C5}$)	

[a] The assignment is given in parantheses below each pair of λ and *f* values. n_{CO} represents a lone-pair of O on CO group(s). n_N represents a lone-pair of N. π_{C6} and π^*_{C6} refer to the bonding and antibonding π on the benzene ring(s), respectively. π_{C5} and π^*_{C5} refer to the bonding and antibonding π on the five-membered ring(s), respectively. π^*_{CO} refers to the antibonding π on CO. π and π^* without a subscript represent the bonding and antibonding π on the whole conjugated π system in **7m**. σ^*_{CH}, σ^*_{CC}, and σ^*_{CN} represent the antibonding σ on C−H, C−C, and C−N bonds, respectively. σ_{CH} and σ_{CC} represent the bonding σ on C−H and C−C bonds, respectively. R indicates that the excited state has Rydberg character.

and 1,2-DATT could be associated with the ninhydrin-like reactions; the formation of pyrrole-like adducts does not produce a color unless they undergo further oxidation processes. Thus, for these two hypotheses, the ninhydrin-like reaction and the pyrrole-like adduct formation, proposed on the basis of extensive experimental studies in the literature, our calculated results support the former. As noted in the Introduction, very recent experimental results based on testing the results of our calculations suggest that species other than ninhydrin could also be involved as the chromogenic marker for the neurotoxic precursors, possibly further oxidized or conjugated pyrrole species.[7] In addition, our calculated results suggest that the formation of the chromophores from 1,2-DAB and 1,2-DATT is likely to follow the same molecular mechanism if they follow a path to ninhydrin-like products.

The Color of the Solution. As only the ninhydrin-like reactions produce visible colors, we can consider which species, **6a**/**8a** or **6b**/**8b**, could be associated with the blue color in neutral solution. As shown in Tables 3 and 4, the neutral species **6b**/**8b** have strong absorptions at ∼480 nm (a typical wavelength for a blue absorption is ∼470 nm[49]). An even stronger absorption is predicted further to the blue at ∼420 and ∼440 nm, for **6b** and **8b**, respectively. Thus, the color of the light absorbed by **6b** will be dominated by the contributions from the absorptions at ∼480 nm and ∼420 nm and for **8b** from the absorptions at ∼480 nm and ∼440 nm, suggesting a blue color or a blue-violet color of the light absorbed by **6b** and **8b**. Since the complementary color of blue/violet is orange/yellow,[50] the corresponding color of the nonabsorbed light should be close to orange or between orange and yellow.

For the deprotonated state, **6a** has a strong absorption predicted at 618 nm, near the typical wavelengths for orange (∼620 nm) and yellow (∼580 nm) colors.[49] The next strong absorption is predicted at ∼406 nm, close to the boundary between the visible violet (∼420 nm) and ultraviolet regions. Hence, the color of the light absorbed by **6a** should be dominated by the absorption at ∼620 nm, with minor contributions from three weaker absorptions between the two strong ones, and it is reasonable to expect an orange or yellow color of the light absorbed by **6a**. The corresponding color of the

(49) Atkins, P. W. *Physical Chemistry*, 3rd ed.; Oxford University Press: New York, 1988; p 432.

(50) Kotz, J. C.; Purcell, K. F. *Chemistry & Chemical Reactivity*; CBS College Publishing: New York, 1987; p 977.

nonabsorbed light should be close to blue or violet. Similarly, **8a** is predicted to have a strong absorption near 630 nm, again followed by three weaker absorptions and another strong absorption at 410 nm; again, **8a** should be blue or violet.

The theoretical results, together with the experimental observation[8,9] of the blue color, strongly suggest that the observed blue color is due to the deprotonated structures **6a** and **8a** that are dominant in the neutral solution. This is consistent with our predicted pK_a value of ~6 based on the MP2 calculations or pK_a value of ~5 based on the DFT calculations. The predicted pK_a value implies that the protonated structures **6b** and **8b** of the chromophores may have significant contributions to the colors at lower pH; in strongly acidic solutions, **6b** and **8b** could be dominant and the colors should be different.

Conclusion

We have carried out a series of ab initio electronic structure calculations on two representative chromogenic aromatic compounds, 1,2-DAB and 1,2-DATT, the metabolites of the neurotoxic aromatic hydrocarbon compounds 1,2-DEB and AETT, and on the products of the reactions of these compounds with amino acids. Three computational approaches, CIS, TD-DFT, and CAS-MP2, have been used to evaluate the electronic excitation energies; they have been validated by calculations on ethylene for which experimental excitation energies are available. It has been shown that the predictions based on both the CAS-MP2 and TD-DFT methods are reliable, and that the CIS calculations can be empirically corrected to obtain a reasonable prediction. The three sets of theoretical results are consistent with each other. All of the calculated results are consistent with a conclusion/prediction that the chromogenic effects of 1,2-DAB (or 1,2-DEB) and 1,2-DATT (or AETT) are not associated with the formation of pyrrole-like adducts but could be associated with products from ninhydrin-like reactions. The pK_a calculations further indicate that if the chromophores are the products of the ninhydrin-like reactions, the species producing the blue color are deprotonated in neutral aqueous solution. The corresponding protonated structures have different colors and could have significant contributions to the colors of the solutions at lower pH. Particularly in acidic solutions, the protonated structures could be dominant and the chromophores could show completely different colors (most likely orange or between orange and yellow). These results do not exclude the possibility of other species based on pyrroles that are highly oxidized or conjugated that might be responsible for the chromogenic properties of the neurotoxic agents under study.

Acknowledgment. This research was performed in the William R. Wiley Environmental Molecular Sciences Laboratory (EMSL) at the PNNL. The EMSL is a national user facility funded by the Office of Biological and Environmental Research in the U.S. Department of Energy. PNNL is a multiprogram national laboratory operated by Battelle Memorial Institute for the U.S. Department of Energy. The work was funded in part by a subcontract to Battelle Pacific Northwest Division from Oregon Health Sciences University under the auspices of a National Institute of Environmental Health Sciences Superfund Basic Research Center Grant No. 5 P42 ES 10338.

Supporting Information Available: Wavelengths λ (nm) and oscillator strengths f calculated by using the TD-DFT method with the B3LYP functional and different basis sets for the first 15 electronic excitations of **5m** (the geometry used was optimized at the B3LYP/6-31+G(d) level); Cartesian coordinates (Å) of the geometries optimized at the B3LYP/6-31G(d) and B3LYP/6-31+G(d) levels; the corresponding total energies in a.u.; the vibrational frequencies (cm^{-1}) calculated at the B3LYP/6-31G(d) level; and the appropriate MP2 energies (PDF). This material is available free of charge via the Internet at http://pubs.acs.org.

JA0113394